

## CHANDRA DETECTION OF DOPPLER SHIFTED X-RAY LINE PROFILES FROM THE WIND OF $\zeta$ PUPPIS (O4f)

J. P. CASSINELLI<sup>1</sup>, N. A. MILLER<sup>1</sup>, W. L. WALDRON<sup>2</sup>, J. J. MACFARLANE<sup>3</sup>, AND D. H. COHEN<sup>3,4</sup>  
*Draft version October 27, 2018*

### ABSTRACT

We report on a 67 ks HETG observation of the optically brightest early O-star,  $\zeta$  Pup (O4 f). Many resolved X-ray lines are seen in the spectra over a wavelength range of 5 to 25 Å. *Chandra* has sufficient spectral resolution to study the velocity structure of isolated X-ray line profiles, and to distinguish the individual forbidden, intercombination, and resonance (*fir*) emission lines in several He-like ions even where the individual components are strongly Doppler broadened. In contrast with X-ray line profiles in other hot stars,  $\zeta$  Pup shows blue-shifted and skewed line profiles, providing the clearest and most direct evidence that the X-ray sources are embedded in the stellar wind. The broader the line, the greater the blueward centroid shift tends to be. The N VII line at 24.78 Å is a special case, showing a flat-topped profile. This indicates it is formed in regions beyond most of the wind attenuation. The sensitivity of the He-like ion *fir* lines to a strong UV radiation field is used to derive the radial distances at which lines of S XV, Si XIII, Mg XI, Ne IX, and O VII originate. The formation radii correspond well with continuum optical depth unity at the wavelength of each line complex, indicating that the X-ray line emission is distributed throughout the stellar wind. However, the S XV emission lines form deeper in the wind than expected from standard wind shock models.

*Subject headings:* X-rays: stars — stars: individual ( $\zeta$  Pup) — stars: early-type — stars: winds, outflows — stars: mass-loss — line: profiles

### 1. INTRODUCTION

The O4f star  $\zeta$  Puppis has for decades been at the cutting edge of research regarding early type stars because of its optical and UV brightness. In addition, because of the low interstellar attenuation,  $\zeta$  Pup has been the prime X-ray target to study soft X-ray emission from O stars. Researchers have looked to this source to settle outstanding controversies about the physical location, quantity, and nature of the hot X-ray emitting plasma on OB stars. In this paper we present the highest resolution X-ray spectrum of  $\zeta$  Pup ever measured and explore the physical mechanism of hot star X-ray production.

Prior to the discovery of X-ray emission from O stars (Harnden et al. 1979; Seward et al. 1979), Cassinelli & Olson (1979) postulated thin base coronal zones as a source for X-rays to explain the observed UV superionization (Lamers & Morton 1976) by way of the Auger effect. The coronal models (Cassinelli & Olson 1979; Waldron 1984) predicted an X-ray absorption at the oxygen K-shell edge larger than that observed with *Einstein* SSS (Cassinelli & Swank 1983) and *BXRT* (Corcoran et al. 1993). These observations, as well as detailed modeling of the superionization profiles (MacFarlane et al. 1993) and lack of detection of the iron “green line” (Baade & Lucy 1987) in  $\zeta$  Pup caused the coronal model to fall out of favor. Increasingly, a consensus formed around a wind-shock picture in which a series of shocks, perhaps related to the line-force instability (Lucy 1982; Owocki, Castor, & Rybicki 1988), causes hot, X-ray emitting gas to be distributed *throughout* the dense stellar wind of  $\zeta$  Pup and

other OB stars. Wind shock models developed by Lucy & White (1980), Feldmeier et al. (1997) and others, consistently failed to predict the high levels of X-ray emission observed in the brightest O stars like  $\zeta$  Pup, leading to the suggestion that perturbations somehow form and propagate up from the photosphere into the wind and drive stronger shocks (Feldmeier 1995; Feldmeier, Puls, & Pauldrach 1997). Broad-band X-ray observations of  $\zeta$  Pup (Corcoran et al. 1993; Hillier et al. 1993) indicate that some wind attenuation is affecting the soft X-ray flux. However with the advent of *Chandra* and *XMM* we can apply, for the first time, diagnostic emission line ratios and measure line profiles to determine the locations and Doppler velocities of X-ray sources in the stellar wind of  $\zeta$  Pup.

### 2. OBSERVATIONS AND CONSTRAINTS FROM HELIUM-LIKE *fir* LINE RATIOS

We obtained a 67 ks *Chandra* High Energy Transmission Grating Spectrometer (HETGS) observation of  $\zeta$  Pup from 2000 Mar 28, 13<sup>h</sup> 31<sup>m</sup> UT to Mar 29, 09<sup>h</sup> 12<sup>m</sup>. The standard pipeline tools were used to reprocess the data with the most recent calibration files available. Line emission is clearly evident in both the high-energy grating (HEG) and the medium-energy grating (MEG). The combined  $\pm 1^{\text{st}}$  order, background-subtracted, HETGS spectra are shown in Figure 1. Triads of He-like ions known as the *fir* (forbidden, intercombination, and resonance) lines (S XV, Si XIII, Mg XI, Ne IX, and O VII) are seen, in addition to isolated Ly $\alpha$  emission lines and numerous L-shell

<sup>1</sup> Astronomy Department, University of Wisconsin, 475 N. Charter St., Madison, WI 53706; cassinelli@astro.wisc.edu, nmiller@astro.wisc.edu

<sup>2</sup> Emergent Information Technologies, Inc., 9314 Largo Drive West, Suite 250, Largo, MD 20774; wayne.waldron@emergent-IT.com

<sup>3</sup> Prism Computational Sciences, 16 N. Carroll St. Madison WI 53703; jjm@prism-cs.com, cohen@prism-cs.com

<sup>4</sup> Department of Physics and Astronomy, Swarthmore College, Swarthmore, PA 19081; dcohen1@swarthmore.edu

lines of iron, especially Fe XVII.

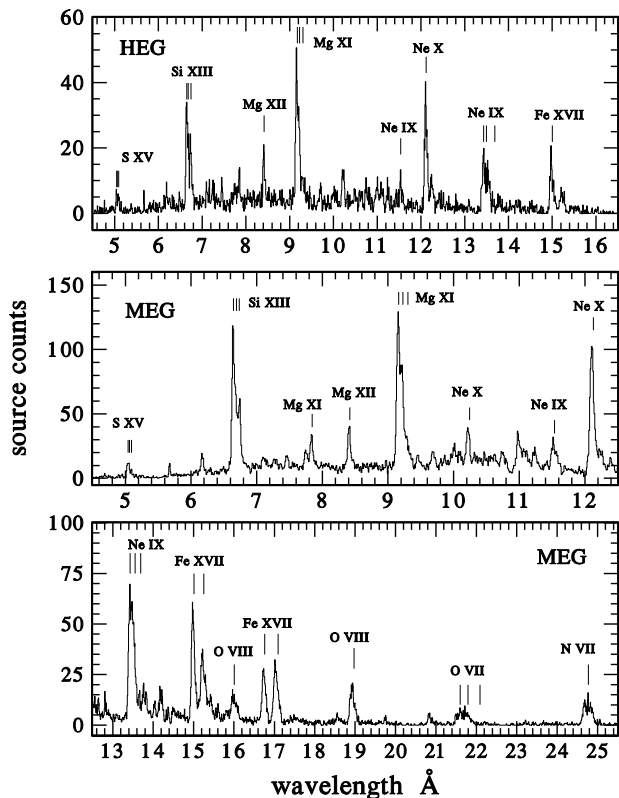


FIG. 1.— Co-added 1<sup>st</sup> order, background subtracted, Chandra HETGS HEG (top panel) and MEG (bottom panels) count spectra of  $\zeta$  Pup. The ions responsible for the strongest line emissions are identified. The bin size is 0.01 Å.

Traditionally, He-like ion  $f/i$  line ratios have been used to derive electron densities of X-ray line emitting regions since the populations of the  $2^3P$  levels are controlled by collisional excitations from the  $2^3S$  levels (Gabriel & Jordan 1969). However, when a strong external UV source is present, the excitation  $2^3S \rightarrow 2^3P$  is predominantly radiative and this means that the  $f/i$  ratio is no longer a density diagnostic, but rather it can be used to determine the strength of the UV radiation field (Blumenthal et al. 1972). The UV wavelengths associated with the radiative excitation are in the range from  $\sim 650$  to  $1650$  Å, where O star UV fluxes are very strong. For  $\zeta$  Pup’s photospheric flux we use a Kurucz (1993) model, assuming  $T_{\text{eff}} = 42000\text{K}$ . Since the  $2^3S \rightarrow 2^3P$  wavelengths are not on the Wien side of the spectrum, the model atmosphere fluxes are relatively well determined.

Waldron & Cassinelli (2001) demonstrated how the observed  $f/i$  line ratios can be used to derive the line formation radii from the geometric dilution of the photospheric radiation field in  $\zeta$  Ori (09.5Ia). Kahn et al. (2001) used a similar approach to derive line formation radii from their *XMM RGS* spectrum of  $\zeta$  Pup. Our *Chandra* HETG spectrum has better resolution at essentially all He-like ion wavelengths and greater sensitivity to the short-wavelength lines (e.g., Si and S) than the *XMM* spectrum. This high resolution is very important for O stars since their X-ray lines show strong broadening. The observed He-like  $f/i$  line ratios are listed in Table 1.

Figure 2a shows the radii derived from our measurements of the He-like  $f/i$  ratios. The radii of line formation are seen to vary from ion to ion, with lines from high nuclear charge ions (Si, S) forming at small radii, and lower nuclear charge ion lines (O, Ne, Mg) forming at larger radii. One might expect the  $f/i$  line complexes for each element to be formed over a range of radii and not just in a thin shell. However, since the line emission is proportional to  $n_e^2$ , the observed emission in each line complex should be dominated by the densest regions (i.e. the smallest radii) from which the line radiation can escape. For  $\zeta$  Ori the  $f/i$  formation locations correlates with the associated radial optical depth unity radius,  $R_1$ . The optical depth is measured through the wind, using the continuum opacity at the wavelength of each triad of  $f/i$  lines. Any line radiation that originates much below  $R_1$  could not be seen by an external observer. The wavelength dependence of  $R_1$  for  $\zeta$  Pup is shown in Figure 2b using a  $\beta$ -law with  $\beta = 0.75$  as the velocity law, the wind absorption cross sections in Waldron et al. (1998), and the stellar parameters of Lamers & Leitherer (1993) ( $R_* = 16 R_\odot$ ,  $\dot{M} = 2.4 \times 10^{-6} M_\odot \text{yr}^{-1}$ , and  $v_\infty = 2200 \text{km s}^{-1}$ ).

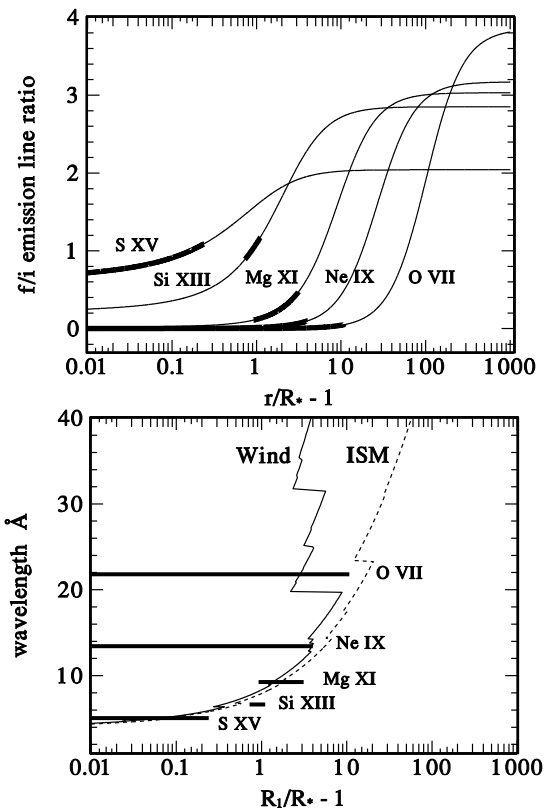


FIG. 2.— The top panel shows the dependence of O VII, Ne IX, Mg XI, Si XIII and S XV  $f/i$  ratios on radius due to the geometric dilution of the UV radiation field. The length of the darkened line for each ion extends over the range of the uncertainty in the  $f/i$  line ratio. The bottom panel gives the radius of wind continuum optical depth unity as a function of wavelength. The dark horizontal lines correspond to the range in radii indicated in the upper panel. For comparison, we also show the optical depth unity radius assuming neutral interstellar medium opacity of Morrison & McCammon (1983).

An inspection of Figure 2 leads to the following conclusions: First, the He-like line formation radii are all consis-

**Table 1:** *fir* ratio measurements

	S XV	Si XIII	Mg XI	Ne IX	O VII
$f/i$	$0.61 \pm 0.48$	$1.03 \pm 0.14$	$0.29 \pm 0.18$	$< 0.1$	$< 0.1$
$r/i$	$0.78 \pm 0.54$	$2.00 \pm 0.25$	$1.53 \pm 0.13$	$1.44 \pm 0.18$	$1.30 \pm 0.6$
$\mathcal{F}_{tot}^a$	0.81	3.06	3.26	5.77	3.56

<sup>a</sup>Total flux of the three lines in  $10^{-13}$  erg cm<sup>-2</sup> s<sup>-1</sup>

tent with their associated  $R_1$  values, as expected from the above argument. Second, the  $f/i$  ratio of S XV indicates that hot plasma exists below  $1.2 R_*$  where the nominal wind velocity is  $< 600$  km s<sup>-1</sup>. Most radiative instability simulations do not show strong shocks this close to the star (Feldmeier 1995, Owocki, Castor, & Rybicki 1988). However, using a velocity jump even half as large as the local wind velocity ( $\Delta v = 300$  km s<sup>-1</sup>) to calculate the shock temperature from  $T = 1.4 \times 10^3 K (\Delta v / 100 \text{ km s}^{-1})^2$ , we obtain a post-shock temperature of 1 MK; too low to produce S XV. Thus, anomalously strong shock jumps are required deep in the wind. A similar conclusion was reached by Waldron & Cassinelli (2001), but for  $\zeta$  Ori the highest ion stage observed was Si XIII instead of the S XV seen here.

### 3. EMISSION LINE PROFILES

The most notable feature observed in our HETG spectrum of  $\zeta$  Pup is the clear presence of blue-shifted X-ray line centroids in all strong lines. This is in contrast with previous *Chandra* O star observations (Schulz et al. 2000; Waldron & Cassinelli 2001) where the lines were broad, symmetric and un-shifted. Although our line widths are comparable to other O-star observations, with HWHM of  $\sim 1000$  km s<sup>-1</sup>, our observation is the first *Chandra* detection of blue-shifted and blueward skewed X-ray line profiles in an O star. Figure 3 displays six  $\zeta$  Pup X-ray lines arranged in order of wavelength. The results for the line fits are given in Table 2. There is an interesting progression that holds for these lines: the centroid shifts are generally larger for the broader lines, indicating a connection between radial location, wind absorption, and the Doppler broadening of the line emission. In Table 4 of their XMM study of  $\zeta$  Pup, Kahn et al. (2001) list blueshifts of the Lyman- $\alpha$  lines of Ne X and O VIII. The blueshifts agree with ours to within 2 sigma, and some of the discrepancy can be attributed to the absolute wavelength calibration uncertainties of the instruments ( $\sim 100$  km s<sup>-1</sup> for the HETG (Chandra X-ray Center (CXC) 2001), see den Herder et al. 2001 for the RGS). The XMM results show the same trend between shift and broadening. The N VII line is an exception to the trend in Table 2 because of its small centroid shift. It is different morphologically from the other lines (also noted by Kahn et al. (2001)). It has a roughly flat-topped profile so we use a box fit instead of a Gaussian to estimate the values for Table 2.

There is a blueward skewness observed in many of the  $\zeta$  Pup lines which is not attributable to the HETGS line response function (CXC 2001). The blue sides of these lines tend to be steeper, while the red sides have a shallower slope. In general, the shape of these lines indicates wind broadening combined with attenuation as would arise from line formation in the marginally thick region near  $R_1$ . MacFarlane et al. (1991), Ignace (2001), and Owocki

& Cohen (2001) demonstrate that emission line profiles can provide important information about the spatial distribution of hot plasma within a stellar wind based both on the velocity-dependence of the intrinsic emission and also on the continuum attenuation across the line. Assuming isotropic emission, the red-shifted emission from the back side of the wind is suppressed by the continuum opacity along the line of sight, while the blue-shifted emission from the near side is less so. This leads to skewed, almost triangular-shaped lines in an optically thick wind.

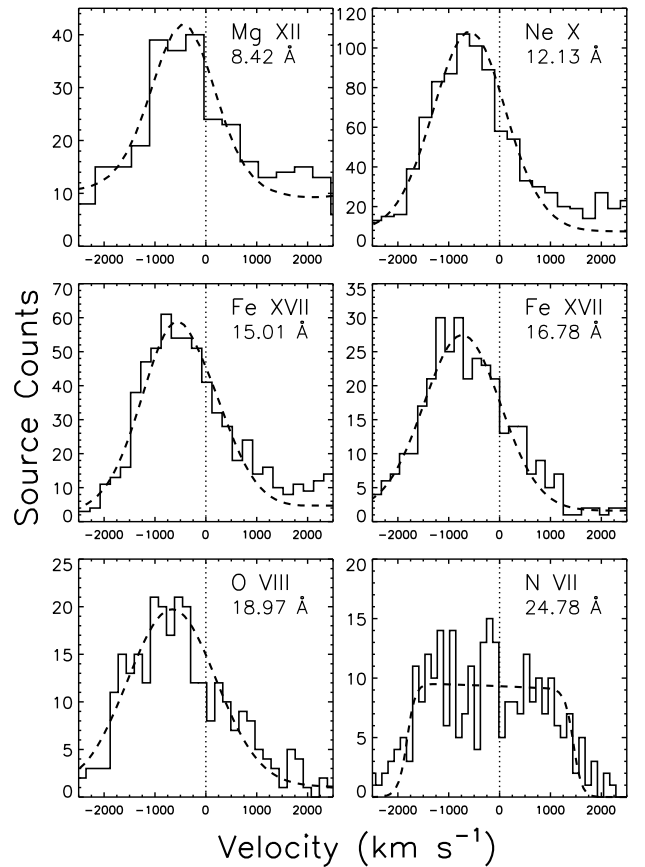


FIG. 3.— Six X-ray line profiles from the  $\zeta$  Pup spectrum (solid) with fits (dashed). The vertical dotted lines indicate the rest wavelengths for these transitions. The first 5 lines were fit with Gaussians while the N VII line was fit with a box function because of its flat-topped shape. All functions shown have been convolved with the instrumental response. These functions are simultaneous fits to the MEG+1 and MEG-1 order spectra but are shown here superimposed on the co-added MEG first order spectrum for the sake of brevity. The data have been binned to 0.01 Å. The fit parameters are given in Table 2.

In the  $\zeta$  Ori HETG spectrum, Waldron & Cassinelli (2001) found that an optically thin model was needed to provide a reasonable fit because the lines were symmetric and un-shifted. This fit required that the assumed mass

**Table 2: Line Profile Widths and Centroid Shifts**

Ion	$\lambda_{\text{rest}}$	$\mathcal{F}_{\text{line}}^{\text{a}}$	Source HWHM	Centroid Shift	$R_1$
	( $\text{\AA}$ )		( $\text{km s}^{-1}$ )	( $\text{km/s}$ )	( $R_*$ )
Mg XII	8.42	0.30	$610 \pm 220$	$-440 \pm 130$	2.8
Ne X	12.13	3.33	$780 \pm 60$	$-570 \pm 50$	4.5
Fe XVII	15.01	4.74	$800 \pm 70$	$-500 \pm 60$	6.0
Fe XVII	16.78	2.24	$850 \pm 130$	$-730 \pm 100$	7.0
O VIII	18.97	3.05	$990 \pm 201$	$-670 \pm 140$	4.0
N VII	24.78	5.02	$1570 \pm 150$	$-120 \pm 150$	4.0

<sup>a</sup>Line flux in  $10^{-13}$  ergs  $\text{cm}^{-2}$   $\text{s}^{-1}$

loss rate for  $\zeta$  Ori be greatly reduced. For  $\zeta$  Pup we have the odd situation that the blueward shift and asymmetric line profiles agree with what has long been expected for hot stars, but this is the first time that it has been so clearly observed in a *Chandra* spectrum for any star. We find that a fit can be made to the line profiles without making a significant reduction in the assumed mass loss rate in contrast with the  $\zeta$  Ori results.

The N VII line profile is different from those of the other ions as can be seen in Figure 3 and Table 2. The Doppler half-width of this line is much greater than any of the other X-ray lines. This velocity of  $1570 \text{ km s}^{-1}$  can be compared with the terminal speed of  $2200 \text{ km s}^{-1}$  determined from UV wind lines. A flat-topped line profile such as this is expected from a fast moving shell source suffering little or no wind attenuation (MacFarlane et al. 1991). Therefore, in contrast with the other observed lines, the NVII profile is probably formed well above its continuum optical depth unity radius.

#### 4. DISCUSSION AND SUMMARY

The *Chandra* HETG emission line spectrum of  $\zeta$  Pup, with its unprecedented resolution (in excess of  $\frac{\Delta\lambda}{\lambda} = 1000$  for some lines) and sensitivity over a wide range of wavelengths, allows us to draw quantitative conclusions about the nature of the X-ray source on this prototypical hot

star. Most importantly, we find that the wind plays an important, observable role in determining the X-ray line profiles of  $\zeta$  Pup, in contrast to results for other stars.

We can begin to constrain the physical processes which lead to the production of the hot, X-ray emitting plasma on this star. Taking all the He-like ions from oxygen through sulfur into account, the correlation between the formation radius of the *fir* lines and the radius at optical depth unity,  $R_1$ , we find evidence for a spatially distributed source of X-rays throughout the expanding wind.

There are two lines of particular interest in the development of future shock models: S XV, and N VII. The shock jump required to produce S XV appears inconsistent with the expected local wind conditions, requiring a post-shock flow velocity of approximately zero. Although this is not impossible for a shock model to reproduce, it places strong constraints on future modeling efforts. The N VII Ly $\alpha$  line may have a shape distinct from the other lines in our spectrum because it is formed in the outer regions of the wind where there is no further acceleration of the X-ray source region and little overlying wind attenuation. This *Chandra* HETG data set provides the most detailed and complete picture to date of an extended distribution of hot plasma embedded within a strong, optically thick stellar wind.

#### REFERENCES

- Baade, D. & Lucy, L. B. 1987, *A&A*, 178, 213  
Blumenthal, G. R., Drake, G. W. F., & Tucker, W. H. 1972, *ApJ*, 172, 205  
Cassinelli, J. P. & Olson, G. L. 1979, *ApJ*, 229, 304  
Cassinelli, J. P. & Swank, J. H. 1983, *ApJ*, 271, 681  
Chandra X-ray Center (CXC) 2000, Chandra Proposers' Observatory Guide, Version 3.0, TD 403.00.003 (Cambridge, MA: CXC), 180, 172  
Corcoran, M. F. et al. 1993, *ApJ*, 412, 792  
den Herder, J. W. et al. 2001, *A&A*, 365, L7  
Feldmeier, A. 1995, *A&A*, 299, 523  
Feldmeier, A., Kudritzki, R. P., Palsa, R., Pauldrach, A. W. A., & Puls, J. 1997, *A&A*, 320, 899  
Feldmeier, A., Puls, J., & Pauldrach, A. W. A. 1997, *A&A*, 322, 878  
Gabriel, A. H. & Jordan, C. 1969, *MNRAS*, 145, 241  
Harnden, F. R. et al. 1979, *ApJ*, 234, L51  
Hillier, D. J., Kudritzki, R. P., Pauldrach, A. W., Baade, D., Cassinelli, J. P., Puls, J., & Schmitt, J. H. M. M. 1993, *A&A*, 276, 117  
Ignace, R. 2001, *ApJL*, 549, 119  
Kahn, S. M., Leutenegger, M. A., Cottam, J., Rauw, G., Vreux, J.-M., den Boggen, A. J. F., Mewe, R., & Güdel, M. 2001, *A&A*, 365, L312  
Kurucz, R. L. 1993, in Peculiar versus Normal Phenomena in A-Type and Related Stars., IAU Colloq. 138, ed. M. M. Dworetzky, F. Castelli, & R. Faraggiana (San Francisco: ASP), 87  
Lamers, H. J. G. L. M. & Leitherer, C. 1993, *ApJ*, 412, 771  
Lamers, H. J. G. L. M. & Morton, D. C. 1976, *ApJS*, 32, 715  
Lucy, L. B. 1982, *ApJ*, 255, 286  
Lucy, L. B. & White, R. L. 1980, *ApJ*, 241, 300  
MacFarlane, J. J., Cassinelli, J. P., Welsh, B. Y., Vedder, P. W., Vallergera, J. V., & Waldron, W. L. 1991, *ApJ*, 380, 564  
MacFarlane, J. J., Waldron, W. L., Corcoran, M. F., Wolff, M. J., Wang, P., & Cassinelli, J. P. 1993, *ApJ*, 419, 813  
Morrison, R. & McCammon, D. 1983, *ApJ*, 270, 119  
Owocki, S. P., Castor, J. I., & Rybicki, G. B. 1988, *ApJ*, 335, 914  
Owocki, S. P., Cohen, D. H. 2001 *ApJ*, submitted, preprint (astro-ph/0101294)  
Schulz, N. S., Canizares, C. R., Huenemoerder, D., & Lee, J. C. 2000, *ApJ*, 545, L135  
Seward, F. D., Forman, W. R., Giacconi, R., Griffiths, R. E., Harnden, F. R., Jones, C., & Pye, J. P. 1979, *ApJ*, 234, L55  
Waldron, W. L. 1984, *ApJ*, 282, 256  
Waldron, W. L., Corcoran, M. F., Drake, S. A., & Smale, A. P. 1998, *ApJS*, 118, 217  
Waldron, W. L., Cassinelli, J. P. 2001 *ApJ*, 548, L45